Astronomy & Astrophysics

LETTER TO THE EDITOR

A hidden reservoir of Fe/FeS in interstellar silicates?

M. Köhler, A. Jones, and N. Ysard

Institut d'Astrophysique Spatiale (IAS), Université Paris-Sud & CNRS, Bât. 121, 91405 Orsay, France
e-mail: mkoehler@ias.u-psud.fr

ABSTRACT

Context. The depletion of iron and sulphur into dust in the interstellar medium and the exact nature of interstellar amorphous silicate grains is still an open question.
Aims. We study the incorporation of iron and sulphur into amorphous silicates of olivine- and pyroxene-types and their effects on the dust spectroscopy and thermal emission.
Methods. We used the Maxwell-Garnett effective-medium theory to construct the optical constants for a mixture of silicates, metallic iron, and iron sulphide. We also studied the effects of iron and iron sulphide in aggregate grains.
Results. Iron sulphide inclusions within amorphous silicates that contain iron metal inclusions show no strong differences in the optical properties of the grains. A mix of amorphous olivine- and pyroxene-type silicate broadens the silicate features. An amorphous carbon mantle with a thickness of 10 nm on the silicate grains leads to an increase in absorption on the short-wavelength side of the $10\,\mu$m silicate band.
Conclusions. The assumption of amorphous olivine-type and pyroxene-type silicates and a 10 nm thick amorphous carbon mantle better matches the interstellar silicate band profiles. Including iron nano-particles leads to an increase in the mid-IR extinction, while up to 5 ppm of sulphur can be incorporated as Fe/FeS nano inclusions into silicate grains without leaving a significant trace of its presence.

Key words. dust, extinction – ISM: abundances

1. Introduction

The depletion of iron into dust is observed in the diffuse interstellar medium (see e.g. Savage & Bohlin 1979; Sofia & Joseph 1995; Jones 2000; Jenkins 2009), but the exact nature of the reservoirs of these elements in dust is unclear. Iron can be included into the silicate structure, but observations show that interstellar silicates are mainly Mg-rich. A more likely possibility is that iron exists in metallic form incorporated into larger particles as inclusions (Costantini et al. 2005; Min et al. 2007; Xiang et al. 2011; Jones et al. 2013). The incorporation of superparamagnetic inclusions in the form of iron (nano-)particles was for example discussed by Jones & Spitzer (1967) to explain the polarisation by dust. This scenario is also supported by laboratory experiments (Davoisne et al. 2006; Djouadi et al. 2007).

The abundance and incorporation of sulphur into dust grains is still an open question. Observations by Ueda et al. (2005) showed that sulphur is undepleted from the gas phase in the diffuse ISM, while it is highly depleted in cold molecular clouds probably by incorporation into dust grains (see also Joseph et al. 1986; Millar & Herbst 1990; Caselli et al. 1994). This would imply that sulphur is incorporated into dust grains in the transition from the diffuse ISM to molecular clouds, which is not understood. Recent studies by U. J. Sofia (priv. comm.) found evidence that sulphur is also depleted in the neutral ISM and that it is therefore an important dust component. It has been assumed that FeS grains are formed in the protoplanetary disks around young stellar objects (Keller et al. 2002) and also as inclusions in glass with embedded metal and sulphides (GEMS; Bradley 1994). Xiang et al. (2011) and Lee et al. (in prep.) also found that the X-ray dust scattering can best be explained with a dust model containing metallic iron with troilite (FeS). Furthermore, work on the STARDUST-collected comet 81P/Wild2 dust indicates a

mix of glassy silicates and Fe-N-S inclusions in the thermally processed grains (Leroux et al. 2009).

For the diffuse ISM, the dust model of Jones et al. (2013) accounts for the Fe depletion by including Fe nano-particles in the grains consist of Mg-rich amorphous silicate. This model considers very small grains (VSGs) and big grains (BGs). The VSGs consist of aromatic amorphous carbon and BGs consist of core-mantle structures with mantles of aromatic amorphous carbon and cores consisting either of aliphatic amorphous carbon or amorphous silicate of forsterite-normative composition[1] with 10% volume Fe metal nano inclusions. These grains are able to reproduce the observed infrared and UV extinction and spectral energy distribution (SED) of the diffuse ISM. Small deviations occur only around the $10-20\,\mu$m silicate features in the infrared extinction, where the observed features are slightly broader and the extinction around $8\,\mu$m is stronger than in the model.

In the model of Jones et al. (2013), the amorphous silicate is assumed to be of forsterite-normative composition. However, many studies discuss the existence of amorphous silicate with olivine- and pyroxene-normative composition. In presolar grains, Nguyen et al. (2007) found silicate grains with both compositions. The dust models reported by Costantini et al. (2005) and Chiar & Tielens (2006) explain observational data by considering both compositions. The study by Demyk et al. (2001) showed that evolutionary processes caused by ion irradiation can change an olivine-type amorphous silicate to an amorphous pyroxene-type silicate. Roskosz et al. (2011) furthermore showed that for annealing at temperatures below the glass transition temperature, pyroxene-type silicate forms preferentially.

---

[1] Amorphous silicate with the same stoichiometry as forsterite. Equivalently for an enstatite-normative composition.
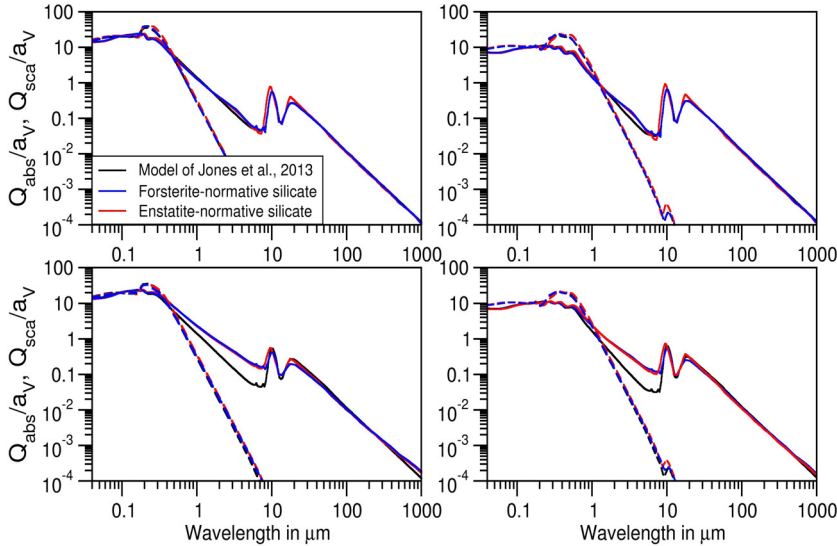
Fig. 1. Q_{abs}/a (solid lines) and Q_{sca}/a (dashed lines) for $a = 0.06\ \mu m$ (*left*) and $a = 0.125\ \mu m$ (*right*) for the silicate BGs from the model of Jones et al. (2013). *Top*: compared with the new silicate grains with Fe and FeS inclusions for amorphous silicate with forsterite-normative composition (blue) and enstatite-normative composition (red). *Bottom*: compared with the same grains with an amorphous-carbon mantle 10 nm thick, instead of 5 nm.

All of these studies suggest that the material composition of the silicate grains is a mixture of amorphous silicates with olivine- and pyroxene-normative compositions.

In this letter, we extend the new dust model of Jones et al. (2013) by modifying the amorphous silicate BG composition. We replace the Fe inclusions with a mixture of Fe and FeS, use amorphous silicate BGs with forsterite- and enstatite-normative composition, and vary the aromatic carbon mantle thickness on the silicate grains. We calculate the optical properties of the grains with this material composition and compare the results with the original model by Jones et al. (2013) and observational data.

2. Material composition and calculations

We used the Maxwell-Garnett effective-medium theory to derive the optical constants of Fe/FeS inclusions within an amorphous silicate matrix. The Maxwell-Garnett mixing rule gives a good approximation of the optical constants of the mixed material. They consist of a mixture of 70% Fe (Ordal et al. 1985, 1988) and of 30% FeS (troilite) (Pollack et al. 1994) by volume. In a second step, we used the Maxwell-Garnett rule again to calculate the optical properties for the mixture of 90% amorphous silicate and 10% Fe plus FeS mixture. We took into account the pair-wise mixing order in the new silicate refractive index data calculation, from most to least refractory materials, as discussed by Jones (2011). For the amorphous silicate, we used the optical constants derived by Scott & Duley (1996) with forsterite- and enstatite-normative composition. We extended the data to longer wavelengths assuming a constant value for n and a decrease of λ^{-1} in the slope for k. These data are consistent with the required Kramers-Kronig relations[2].

Subsequently, we used the BHCOAT routine (Bohren & Huffman 1983) to derive the optical properties of the core-mantle grains. The core consists of the mixture of amorphous silicate, either of forsterite- or enstatite-normative composition, and nano-inclusions of the Fe/FeS mixture. The mantle consists of aromatic-rich amorphous carbon (band gap energy $E_g = 0.1$ eV). The mantle thickness was first assumed to be 5 nm as described by Jones et al. (2013). Then in a second calculation we increased the mantle thickness to 10 nm. The optical properties

for these composite particles were calculated for 30 particle sizes between 0.03 and 5000 μm to cover the full size distribution.

We used DustEM[3] (Compiègne et al. 2011) to calculate the grain temperatures, extinction, and SED. First, we considered the model of Jones et al. (2013) with three types of grains: VSGs of aromatic-rich amorphous carbon up to 20 nm in size, larger grains (BGs) of amorphous carbon with core-mantle structure, where the core consists of aliphatic-rich amorphous carbon and the aromatic-rich amorphous carbon mantle has a thickness of 20 nm, and large grains (BGs) of forsterite-type amorphous silicate with Fe metal nano inclusions with a 5 nm mantle of aromatic-rich amorphous carbon. Second, we considered our model with two types of amorphous silicate grains with Fe/FeS inclusions as described above, where we assumed that half of the amorphous silicate grains consist of forsterite-normative composition and the other half of enstatite-normative composition. We furthermore varied the mantle thickness of these silicate grains. We assumed the same size distribution as described in Jones et al. (2013) and used the interstellar radiation field (ISRF) described by Mathis (1990) to heat the grains.

In denser regions of the ISM, the individual grains start to coagulate into aggregates. To understand the influence of the changes on the material composition when coagulating the grains, we carried out calculations using the discrete-dipole approximation (DDA, Purcell & Pennypacker 1973; Draine 1988; Draine & Flatau 2010). Aggregates are formed of four BGs and 4000 VSGs. Three BGs consist of amorphous silicate and one BG of amorphous carbon. Following the original model of Jones et al. (2013), all amorphous silicate BGs have a forsterite-normative compositions and Fe nano-inclusions. For the new silicates and Fe/FeS inclusions, we replaced the three BGs of amorphous silicate either by two BGs of amorphous silicate with forsterite-normative composition and one BG of amorphous silicate with enstatite-normative composition (model 1) or by one BG of amorphous silicate with forsterite-normative composition and two BGs of amorphous silicate with enstatite-normative composition (model 2). Both types of silicate have 10% Fe/FeS nano inclusions, as described above. The method and calculations to derive the optical properties of these aggregates are described in detail in Köhler et al. (in prep.).

---

[2] The new silicate data are available on request from the authors.

[3] DustEM is a publicly available numerical tool to calculate, for example, the SED, the extinction and the grain temperature distribution for dust in the ISM, available at http://www.ias.u-psud.fr/DUSTEM/
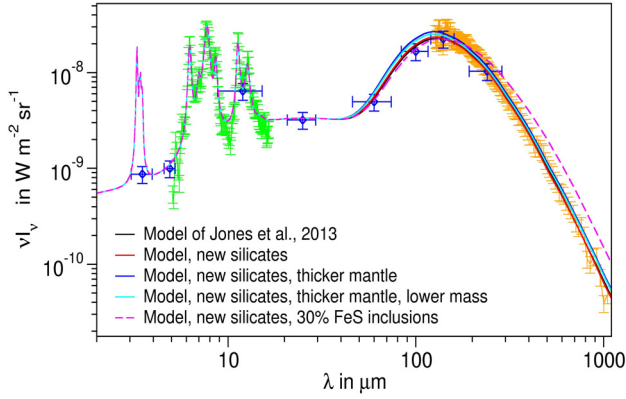
Fig. 2. Dust SED of the diffuse ISM modelled with the original model of Jones et al. (2013) compared with the SED of the model with new amorphous silicate BGs. Included are observations of the diffuse ISM from ISO ISOCAM/CVF (green curve), COBE FIRAS (orange curve), and COBE DIRBE (blue symbols) (see also Compiègne et al. 2011).
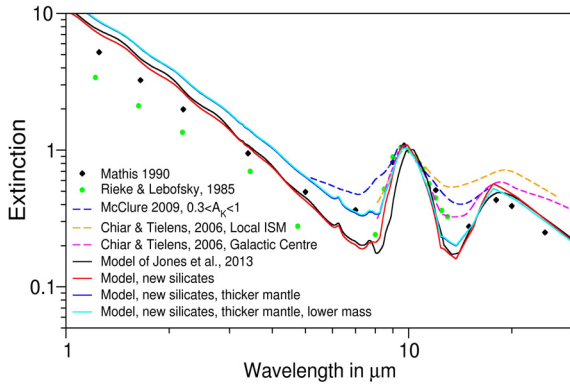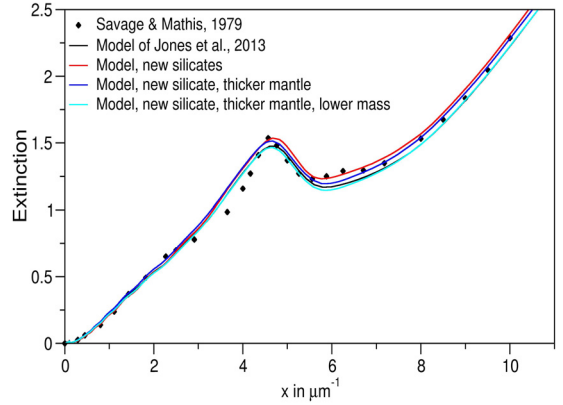

Fig. 3. Extinction of the original model of Jones et al. (2013) and of the modified model with new amorphous silicate BGs, normalised at 10 μm, compared with observational data.

3. Results

In Fig. 1 we show the absorption and scattering coefficients, Q_{abs} and Q_{sca}, divided by the grain radius, a, of 0.064 μm (left) and 0.125 μm (right) for the amorphous silicate grains of the model of Jones et al. (2013) and for the new amorphous silicate grains of forsterite and enstatite-normative composition with Fe/FeS inclusions. The amorphous-carbon mantle is 5 nm (top) and 10 nm thick (bottom). The results show only small differences in Q_{sca}/a. For a given mantle thickness, we note only small differences in Q_{abs}/a between the model of Jones et al. (2013) and the modified model with forsterite-normative amorphous silicate grains. For the amorphous silicate grains of enstatite-normative composition the peak of the silicate features are shifted to shorter wavelengths and the 18 μm feature is more pronounced. The FeS in the Fe/FeS inclusions leads to a slight increase in the absorption in the 3−4 μm region. Increasing the mantle thickness leads to an increase in Q_{abs}/a in the 1−10 μm region compared with the original results of the model of Jones et al. (2013), which results in a weakening of the very broad FeS feature.

The SED and extinction of the diffuse ISM calculated with DustEM are shown in Figs. 2–4. Compared with the original model (black curves), we find only small differences in the SED for the new model (red curves) with the same mantle thickness. Only for a thick mantle (10 nm) (blue curve) do we find a small increase in emission in the far-IR and a shift of the maximum to
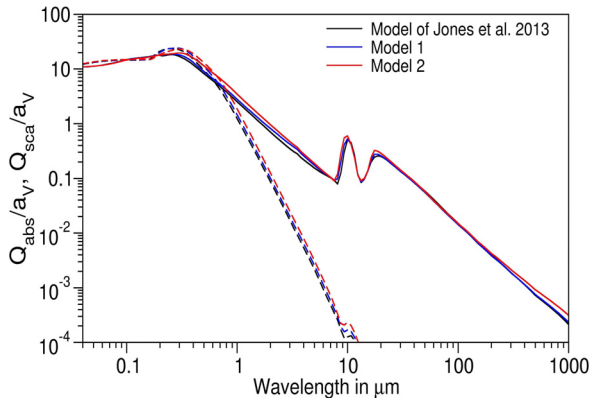

Fig. 4. Extinction in the UV of the original model of Jones et al. (2013) and of the modified models.

shorter wavelengths, indicating an increase in grain temperature. Reducing the abundance of silicate from $M_{dust}/M_H = 5.8 \times 10^{-3}$ to $M_{dust}/M_H = 5.4 \times 10^{-3}$, where each amorphous silicate provides half of the mass and changing the parameter, a_0, of the logarithmic normal size distribution as described in Jones et al. (2013) from 8.0 to 7.0, we again find good agreement with observations (cyan curve). This requires a silicate element abundance of 31 ppm, which agrees with the assumed abundances in dust (see e.g. Compiègne et al. 2011).

In extinction, we find a broadening of the 10 μm silicate feature caused by the mix of olivine- and pyroxene-type amorphous silicate in the new model (red curve) compared with the original model of Jones et al. (2013) (black curve, Fig. 3), which agrees well with the observational data from Rieke & Lebofsky (1985), Mathis (1990), and Chiar & Tielens (2006). The addition of Fe/FeS inclusions into silicates does not change the extinction curve. The original model and the new model, with a mantle thickness of 5 nm, do not explain the slope of the extinction reported by Mathis (1990) in the 1−10 μm region. A mantle of 10 nm leads to an increase in extinction at these wavelengths, which better explains these observations (see blue and cyan curve in Fig. 3, where data are normalised at 10 μm). However, compared with other observations, for example those by McClure (2009), and at wavelength ranges outside the silicate features we note larger deviations, which cannot be explained with our model. We will discuss this extinction problem in detail in a future paper.

Figure 4 shows that differences in the UV bump and FUV extinction are minimal since they are caused by the VSGs, which we did not change compared to the original model. The results of all of the models agree well with the extinction curve of Savage & Mathis (1979).

The FeS inclusions in the silicate grains require an S abundance of 2 ppm (cosmic abundance ∼16 ppm). We find that varying the Fe/FeS mixture up to 1:1 (3 ppm of S) results in only small deviations in the SED and extinction. Replacing the Fe/FeS inclusions by pure FeS inclusions (5 ppm of S) shows small deviations in the SED, where the peak shifts to longer wavelengths (decrease in temperature) and the emission at long wavelengths increases. Increasing the volume of FeS inclusions to 30% (13 ppm of S) leads to an increase in the SED at long wavelengths (see pink dashed curve in Fig. 2). Increasing the amount of Fe/FeS inclusions to 20% (3 ppm of S and ∼60 ppm of Fe) results in an increase in the extinction in the 1−8 μm region. However, such a large increase in the volume fraction of Fe/FeS inclusions is not possible because this is incompatible with the available Fe abundances (cosmic abundance ∼32 ppm).

Fig. 5. Q_{abs}/a_V (solid lines) and Q_{sca}/a_V (dashed lines) for aggregates formed with grains from the original model of Jones et al. (2013) and for aggregates of models 1 and 2 formed with grains consisting of the new amorphous silicate BGs.

The UV extinction is mainly independent of these differences and we only find small differences in the UV extinction bump.

Pre-solar grains contain SiC with an abundance of ∼20 ppm. Including these grains (with an aromatic-rich carbon mantle of 5 nm thickness) does not lead to strong differences in the SED. In extinction we find small differences between 2 and 8 μm and a slight broadening of the silicate features between 10 and 14 μm.

In Fig. 5 we present the results for aggregates consisting of the individual grains from the original model by Jones et al. (2013) (black curve) and for aggregates consisting of the individual grains from the new amorphous silicate composition as described above (blue curve for model 1 and red curve for model 2). The optical properties Q_{abs}/a_V and Q_{sca}/a_V are shown for one aggregate size, $a_V = 0.101$ μm, which is the radius of the volume-equivalent sphere of four single BGs of 0.06 μm and of 4000 VSGs of 3.5 nm in size. The values for Q_{sca}/a_V are slightly higher for model 2 than model 1. For model 2 the differences in Q_{abs}/a_V are larger than for model 1, especially in the 10 and 20 μm silicate features, which are also slightly broader for model 2, and in the 0.3−6 μm region. In the V, J, H, and K band, the increase in Q_{abs} for model 2 is a factor of around 1.4. Whether this effect is grain-size dependent and how it influences the extinction will be discussed in a follow-up paper. At long wavelengths model 1 does not show strong deviations from the original model by Jones et al. (2013), while model 2 shows slightly higher values and a slightly flatter slope. In summary, for both aggregates and single grains the differences in Q_{abs} and Q_{sca} are small. In both cases, the mid-IR silicate features are broader, which agrees with observations.

4. Summary and conclusions

We have extended the dust model of Jones et al. (2013) by introducing a mix of amorphous olivine- and pyroxene-type silicate grains with Fe/FeS nano-inclusions and by considering the effects of a thicker carbonaceous mantle.

Adopting a 1:1 mix of amorphous olivine- and pyroxene-type silicates leads to broader silicate features and better agreement with the observed band profiles, in accord with earlier interpretations and the composition of pre-solar silicate grains.

FeS nano-inclusions do not significantly affect the optical properties of amorphous olivine- and pyroxene-type silicate grains/aggregates with Fe metal inclusions. We conclude that such composite grains can explain the nature of iron in interstellar dust, that is, as metal inclusions in amorphous silicate, and can provide a reservoir for S (as FeS) in the ISM. In particular, we note that FeS inclusions (up to 5 ppm of S) into silicate dust would deplete up to 1/3 of the cosmic S in the ISM in an almost undetectable form. A larger volume fraction of FeS inclusions results in variations in the SED that appear to be consistent with observations (Planck Collaboration XI 2014).

We also showed that increasing the carbon mantle thickness to 10 nm instead of 5 nm enhances the extinction in the 3−10 μm region, which appears to agree better with some observational data. In future studies we plan to investigate this and all of the above effects in more detail.

References

Bohren, C., & Huffman, D. 1983, Absorption and Scattering of Light by Small Particles (New York: Wiley and Sons)
Bradley, J. P. 1994, Science, 265, 925
Caselli, P., Hasegawa, T. I., & Herbst, E. 1994, ApJ, 421, 206
Chiar, J. E., & Tielens, A. G. G. M. 2006, ApJ, 637, 774
Compiègne, M., Verstraete, L., Jones, A., et al. 2011, A&A, 525, A103
Costantini, E., Freyberg, M. J., & Predehl, P. 2005, A&A, 444, 187
Davoisne, C., Djouadi, Z., Leroux, H., et al. 2006, A&A, 448, L1
Demyk, K., Carrez, P., Leroux, H., et al. 2001, A&A, 368, L38
Djouadi, Z., Gattacceca, J., D'Hendecourt, L., et al. 2007, A&A, 468, L9
Draine, B. 1988, ApJ, 333, 848
Draine, B. T., & Flatau, P. J. 2010, unpublished [arXiv:1002.1505]
Jenkins, E. B. 2009, ApJ, 700, 1299
Jones, A. P. 2000, J. Geophys. Res., 105, 10257
Jones, A. P. 2011, A&A, 528, A98
Jones, R. V., & Spitzer, Jr., L. 1967, ApJ, 147, 943
Jones, A. P., Fanciullo, L., Köhler, M., et al. 2013, A&A, 558, A62
Joseph, C. L., Snow, Jr., T. P., Seab, C. G., & Crutcher, R. M. 1986, ApJ, 309, 771
Keller, L. P., Hony, S., Bradley, J. P., et al. 2002, Nature, 417, 148
Leroux, H., Roskosz, M., & Jacob, D. 2009, Geochim. Cosmochim. Acta, 73, 767
Mathis, J. S. 1990, ARA&A, 28, 37
McClure, M. 2009, ApJ, 693, L81
Millar, T. J., & Herbst, E. 1990, A&A, 231, 466
Min, M., Waters, L. B. F. M., de Koter, A., et al. 2007, A&A, 462, 667
Nguyen, A. N., Stadermann, F. J., Zinner, E., et al. 2007, ApJ, 656, 1223
Ordal, M. A., Bell, R. J., Alexander, Jr., R. W., Long, L. L., & Querry, M. R. 1985, Applied Optics, 24, 4493
Ordal, M. A., Bell, R. J., Alexander, Jr., R. W., Newquist, L. A., & Querry, M. R. 1988, Applied Optics, 27, 1203
Planck Collaboration XI 2014, A&A, in press [arXiv:1312.1300]
Pollack, J. B., Hollenbach, D., Beckwith, S., et al. 1994, ApJ, 421, 615
Purcell, E. M., & Pennypacker, C. R. 1973, ApJ, 186, 705
Rieke, G. H., & Lebofsky, M. J. 1985, ApJ, 288, 618
Roskosz, M., Gillot, J., Capet, F., Roussel, P., & Leroux, H. 2011, A&A, 529, A111
Savage, B. D., & Bohlin, R. C. 1979, ApJ, 229, 136
Savage, B. D., & Mathis, J. S. 1979, ARA&A, 17, 73
Scott, A., & Duley, W. W. 1996, ApJS, 105, 401
Sofia, U. J., & Joseph, C. L. 1995, in American Astronomical Society Meeting Abstracts #186, BAAS, 27, 860
Ueda, Y., Mitsuda, K., Murakami, H., & Matsushita, K. 2005, ApJ, 620, 274
Xiang, J., Lee, J. C., Nowak, M. A., & Wilms, J. 2011, ApJ, 738, 78